Research Article

Texture Directionality-Based Digital Watermarking in Nonsubsample Shearlet Domain

Jian Zhao,[1] Shuaishuai Fan,[1] Jian Jia,[1,2] Shunli Zhang,[1] Bo Jiang,[1] Wensheng Xu,[1] and Wanru Zhang[1]

[1]*School of Information Science and Technology, Northwest University, Xi'an 710127, China*
[2]*School of Mathematics, Northwest University, Xi'an 710127, China*

Correspondence should be addressed to Jian Jia; jiajian@nwu.edu.cn

Digital watermarking is a technique used to protect an author's copyright and has become widespread due to the rapid development of multimedia technologies. In this paper, a novel watermarking algorithm using the nonsubsample shearlet transform is proposed, which combines the directional edge features of an image. A shearlet provides an optimal multiresolution and multidirectional representation of an image based on distributed discontinuities such as edges, which ensures that the embedded watermark does not blur the image. In the proposed algorithm, the nonsubsample shearlet transform is used to decompose the cover image into directional subbands, where different directional subbands represent different directional and textured features. The subband whose texture directionality is strongest is selected to carry the watermark and is thus suitable for the human visual system. Next, singular value decomposition is performed on the selected subband image. Finally, the watermark is embedded in the singular value matrix, which is beneficial for the watermarking robustness and invisibility. In comparison with related watermarking algorithms based on discrete wavelet transforms and nonsubsample contourlet transform domains, experimental results demonstrate that the proposed scheme is highly robust against scaling, cropping, and compression.

1. Introduction

Given the rapid development of digital data and associated technologies, copyright protection of multimedia has become a challenging problem. In order to protect an author's ownership, the method of digital watermarking (a digital data hiding technique) provides an effective solution. A good digital watermarking algorithm must ensure that (1) the embedded watermark is visually imperceptible, (2) the reconstructed watermarked image has good visual quality, and (3) the watermark is resilient to attacks. In other words, a watermarking technique should resist watermark degradation due to common signal processing and geometric attacks.

A watermarking algorithm is regarded optimal if the scheme can balance the quality index of watermark robustness, imperceptibility, and capacity as proposed by Fridrich [1]. Watermarking can be performed in either the spatial domain (e.g., least significant bit) [2] or the transform domain

(e.g., discrete Fourier transform (DFT) or discrete cosine transform (DCT)) [3, 4]. Moreover, the discrete wavelet transform (DWT) [5, 6] has the ability to capture 1D signal characteristics at different scales or resolutions, which makes the method widely applicable for image processing applications such as denoising and compression. However, DWT is unable to effectively represent multidimensional signals, and its limited directional filtering restricts watermarking capacity.

In order to overcome the limitations of the wavelet transform, several multiscale geometric analysis (MGA) tools such as ridgelet, directionlet, and contourlet transforms have been developed and successfully applied in image processing applications [7–12]. Shearlet, a multiresolution method, provides a tremendously effective representation of images containing edges [13, 14] and is widely used in watermarking algorithms [15–18]. Spread spectrum image watermarking in the discrete shearlet domain [15] employs the multiresolution

representation characteristics of the DST to facilitate texture modeling for a given image. Zhao et al. [16] proposed a watermarking scheme based on the extended shearlet, where the watermark was embedded into the subband with the largest information entropy. Based on previous studies [17], a watermarking algorithm was proposed using the shearlet transform and bidiagonal singular value to achieve balance between robustness and imperceptibility.

In this paper, a nonsubsample shearlet transform (NSST), along with a combination of Laplace and shear filters, is used to decompose an image into different scales and directional subbands. The watermark can then be embedded into a special directional subband that achieves the best result. The proposed watermarking scheme has high robustness and imperceptibility depending on texture directionality in the NSST domain. The texture of an image with strong directionality reflects the contours and directional edges of the image, and the directional filter bank (DFB) of the NSST can effectively capture high-frequency content. The selection of a subband with strong texture directionality plays a significant role in the embedding and extraction steps of the watermarking algorithm.

The rest of this paper is organized as follows. Basic shearlet theory and related data are presented in Section 2. The proposed novel watermarking embedding and detection scheme is presented in Section 3. Experimental results are provided and discussed in Section 4, while important findings and conclusions are summarized in Section 5.

2. Correlation with Basic Theory

2.1. Shearlet Transform. Shearlets, or composite wavelets, provide an effective way to achieve a sparse directional image representation based on affine transformations and a combination of geometry and multiple scales. For dimension $n = 2$, the affine system with composite dilations is described by

$$\Lambda_{AB} \left\{ \psi_{a,s,t} (x) = |\det A|^{a/2} \psi \left(B^s A^a x - t \right) : a, s \in R, \ t \in R^2 \right\},$$ (1)

where $\psi \in L^2(R^2)$, **A** and **B** are 2×2 invertible matrices, and $|\det B| = 1$. When **A** is the set $A_a = (a, 0; 0, \sqrt{a})$ $(a > 0)$, it is related to the scale transform, and the shear matrices $B_s = (1, s; 0, 1)$ are related to the area-preserving geometrical transform. The transform is described as [14]

$$SH (\psi) = \begin{cases} \psi_{a,s,t} (x) = a^{-3/4} \psi \left(A_a^{-1} B_s^{-1} x - t \right) \\ \\ = a^{-3/4} \psi \left(\begin{pmatrix} \dfrac{1}{a} & -\dfrac{s}{a} \\ 0 & \dfrac{1}{\sqrt{a}} \end{pmatrix} x - t \right), \ a > 0, \ s \end{cases}$$

$$\in \left[-\left(1 + a^{1/2}\right), 1 + a^{1/2} \right], \ t \in R^2 \Bigg\}.$$ (2)

We select ψ such that

$$\widehat{\psi} (\xi) = \widehat{\psi} (\xi_1, \xi_2) = \widehat{\psi}_1 (\xi_1) \widehat{\psi}_2 \left(\frac{\xi_2}{\xi_1} \right),$$ (3)

where $\widehat{\psi}_1$ is a continuous wavelet for which $\widehat{\psi}_1 \in C^\infty(R)$ with $\widehat{\psi}_1 \subset [-2, 1/2] \cup [1/2, 2]$ and $\widehat{\psi}_2$ is selected to satisfy $\widehat{\psi}_2 \in C^\infty(R)$ with $\widehat{\psi}_2 \subset [-1, 1]$, $\widehat{\psi}_2 > 0$ on $(-1, 1)$, and $\|\widehat{\psi}_2\| = 1$. Under this assumption, the associated continuous shearlet transform of $f \in L^2(R^2)$ is defined as

$$SH_f (a, s, t) = \langle f, \psi_{a,s,t} \rangle.$$ (4)

Sampling $SH(\psi)$ on the discrete set of a, s, and t is done as follows [13, 16]:

$$a_l = 2^l \quad (l \in Z),$$
$$s_j = j * a_l^{1/2} = j * 2^{j/2} \quad (k \in Z).$$ (5)

The associated discrete shearlet transform is described by

$$\left\{ \psi_{j,l,k}^{(d)} (x) = |\det A_d|^{j/2} \psi \left(B_d^l A_d^j x - k \right) : j \geq 0, \right.$$
$$\left. -\left[2^{j/2} \right] \leq l \leq \left[2^{j/2} \right], \ k \in Z^2, \ d = 0, 1 \right\}.$$ (6)

2.2. Nonsubsample Shearlet Transform (NSST). The nonsubsample shearlet transform (NSST) is composed of the nonsubsample Laplacian pyramid transform and several different combinations of shearing filters. Figure 1(a) shows the flowchart for a nonsubsample shearlet where the Laplacian pyramid (LP) is used to capture point discontinuities and the directional filter bank (DFB) is used to link point discontinuities into linear structures. The DFB is designed to capture high-frequency content such as directional edges. An example of a frequency partition is shown in Figure 1(b).

A test image *(zoneplate)* is decomposed by NSST as shown in Figure 2. For LP decomposition, an approximate image is generated, and after DFB, 8 and 16 different directional subbands are obtained in the respective scale.

As observed in Figure 2, image directionality is strongly apparent after the shearlet transform. Different directional subbands represent the directional information related to different image details. Finally, the subband with the maximum texture directionality is selected for watermark embedding.

2.3. Singular Value Decomposition (SVD). Singular value decomposition (SVD) is a numerical statistical analysis tool that is used to effectively deal with matrices. Assume that an
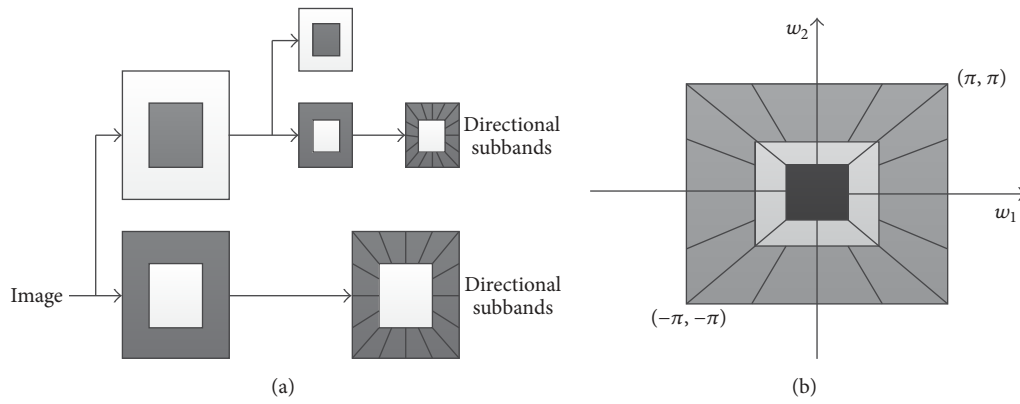
(a)

(b)

FIGURE 1: Diagram of shearlet transform: (a) illustration of succession of Laplacian and directional filtering and (b) example of frequencies by the shearlet transform.
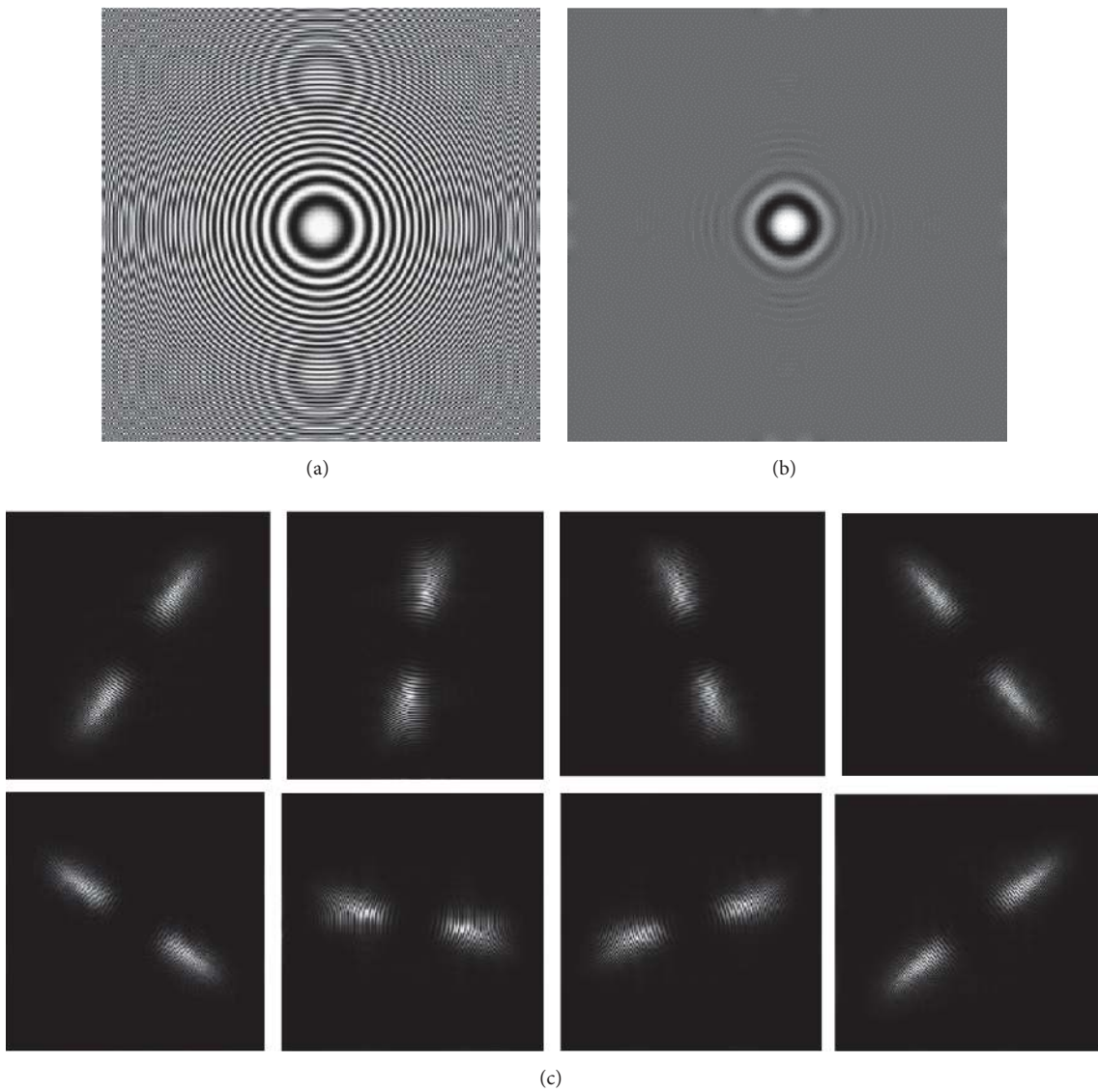

(a)

(b)

(c)

FIGURE 2: Shearlet decomposition of *zoneplate* image: (a) *zoneplate*, (b) approximate NSST coefficients, and (c) detailed coefficients.

TABLE 1: Values of texture directionality.

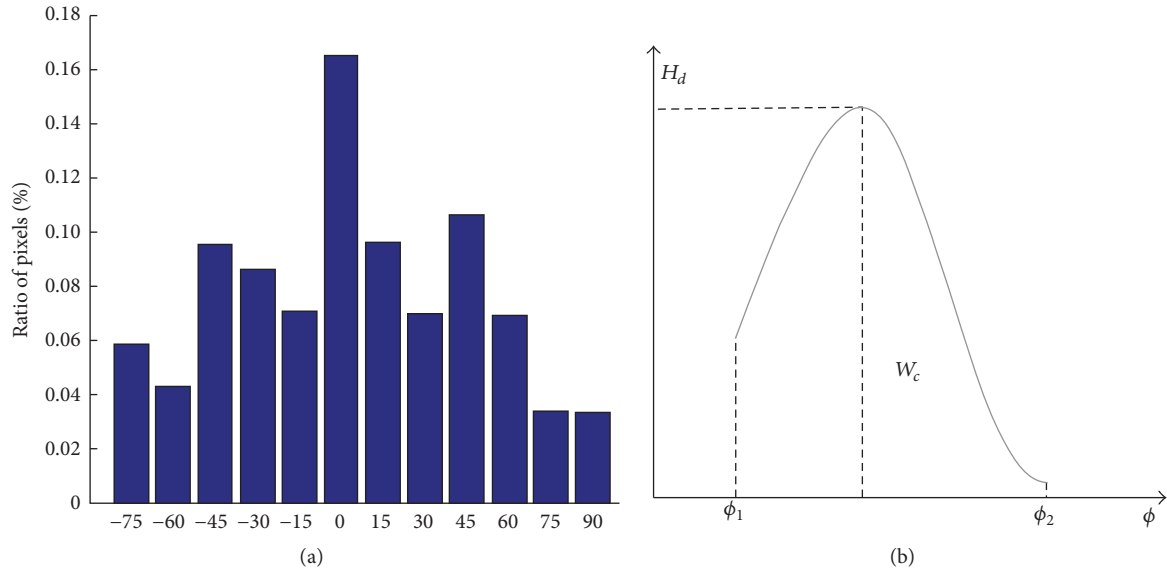| Image	D1	D2	D3	D4	D5	D6	D7	D8
Directionality	0.3135	0.2673	0.2103	0.3321	0.1964	0.3111	0.3247	0.3007

FIGURE 3: Directionality of texture: (a) direction edge histogram of Lena and (b) a peak in the edge histogram.

image is a nonnegative matrix. The singular value decomposition of matrix $\mathbf{AA}$ is defined as

$$\mathbf{AA} = USV^T$$

$$= [u_1, u_2, \ldots, u_n] \begin{bmatrix} \sigma_1 & & & \\ & \sigma_2 & & \\ & & \ddots & \\ & & & \sigma_n \end{bmatrix} [v_1, v_2, \ldots, v_n]^T \quad (7)$$

$$= \sum_{i=1}^{n} \sigma_i u_i v_i,$$

where $U \in R^{m*n}$ and $V \in R^{m*n}$ are orthogonal matrices, $S \in R^{m*n}$ is a diagonal matrix, and V^T is the transpose of $\mathbf{V}$. The diagonal elements of $\mathbf{S}$ satisfy $\sigma_1 \geq \cdots \geq \sigma_r \geq \sigma_{r+1} = \cdots = \sigma_n = 0$, where r is the rank of $\mathbf{AA}$ and is equal to the number of nonnegative singular values.

An important property of SVD is that the singular values (SVs) of an image possess significant stability because these values do not vary rapidly with small image perturbations. Therefore, a watermark embedded in a singular matrix exhibits high robustness [19–23].

3. Proposed Watermarking Scheme

3.1. Texture Directionality. Texture is a property that exists in many areas. In the scope of image processing, texture denotes a trend or pattern that reflects a change in the intensity and direction of image pixels. Directionality is one of the

most significant characteristic features. This paper proposes a method based on statistical measurements for calculating image directionality from the directional histogram [24, 25].

For a given image pixel, if the outputs of the horizontal and vertical edge operators are ΔH and ΔV, respectively, then the corresponding gradient vector ΔG is

$$|\Delta G| = \frac{|\Delta H| + |\Delta V|}{2}$$

$$\theta = \frac{\pi}{2} + \tan^{-1}\left(\frac{\Delta V}{\Delta H}\right) \quad 0 \leq \theta \leq 180°. \quad (8)$$

Thus, the modulus $|\Delta G|$ and angle θ of the vector are obtained. The direction edge histogram H_d is then calculated by quantizing θ and counting the ratio of effective pixels. A direction edge histogram for the Lena test image is shown in Figure 3(a).

Assuming that the variation trend denotes n peaks in the histogram, Figure 3(b) shows one of these peaks. Let w_c be a collection of bins from the previous valley ϕ_1 to the next valley ϕ_2 for each peak p, and let λ_p be the angle position of the peak. $H_d(\lambda)$ is the bin height at angle position λ. Texture directionality is calculated as [24]

$$f_{\text{dir}} = \sum_{P}^{n} \sum_{\lambda \in w_c} \left(\lambda - \lambda_p\right)^2 H_d(\lambda). \quad (9)$$

The image texture direction is computed as a numerical value based on the above description. Figure 4 shows reconstructed images for eight shearlet direction coefficients, and the corresponding texture directionality values are shown in Table 1. The fourth subband with the largest value represents

(a)

D1   D2   D3   D4
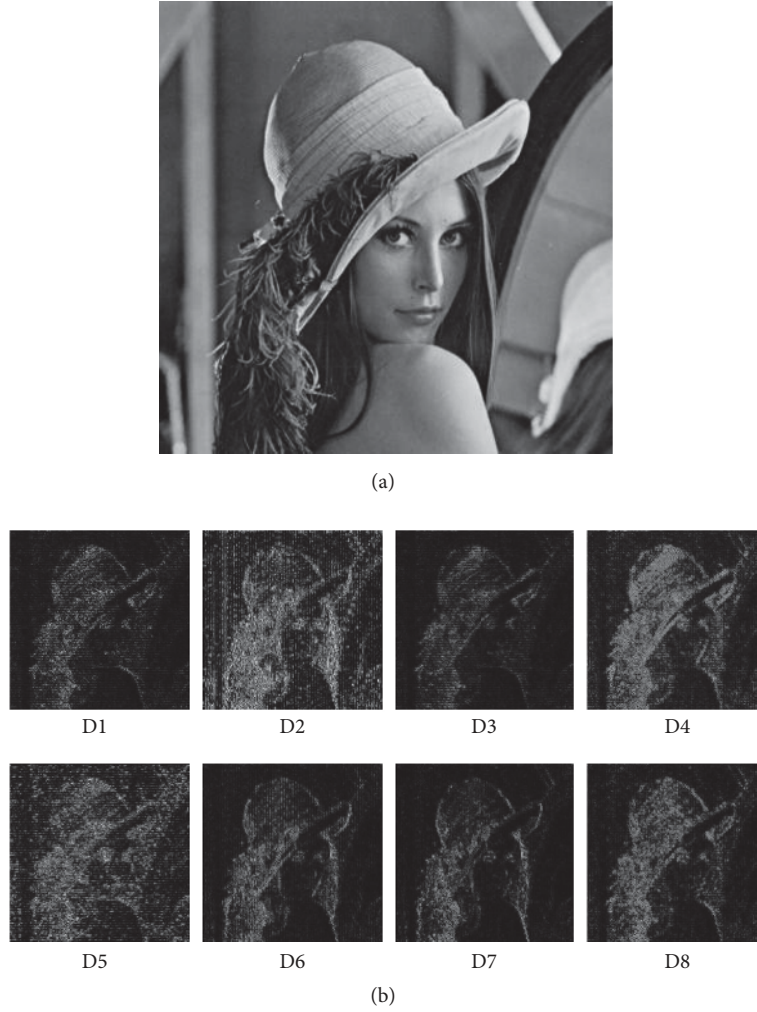
D5   D6   D7   D8

(b)

FIGURE 4: (a) *Lena* test image. (b) Eight reconstructed images (D1–D8) of shearlet direction coefficients.

strong directionality and is selected to carry the watermark. The texture of an image with strong directionality reflects the contours and directional edges, and the directional filter bank of NSST can effectively capture high-frequency content. Further, due to its scale-invariant nature, stability does not change with scaling, rotation, or noise attacks. Thus, this property is an advantage for watermark hiding and robustness.

3.2. Proposed Watermarking Algorithm. Consider that the cover (host) image is a grayscale image $f(i, j)$ with size $N \times N$, while the watermark is a binary image **W** with size $M \times M$ and elements $w(i, j)$. The selection of a suitable location, effective coefficients to embed, and the embedding mechanism is of crucial importance in any watermarking scheme. In the proposed scheme, we select the eighth directional subband of level 3 with maximum directionality. This suggests that the subband has significant values to indicate the presence of

directional edges, which contribute to watermark imperceptibility. Details on the embedding and extraction process are provided below.

3.2.1. Watermark Embedding

Step 1. In order to increase watermarking security, the encrypted watermark W^* is obtained through the Arnold scrambling transform:

$$W^* = \text{arnold}\,(W, \text{key})\,, \tag{10}$$

where key represents scrambling times and is held to the decrypted watermark as the secret key.

Step 2. A host image with size 512×512 is decomposed by 2-level NSST. An approximation image and directional subbands $S_{i,j}$ ($1 \leq i \leq 2$, $1 \leq j \leq 2^{k_i}$) with size 512×512 are obtained.

TABLE 2: The relationship between α and watermarking imperceptibility.

α	0.05	0.2	0.5	0.7	1
SSIM	1.0000	1.0000	0.9999	0.9998	0.9973

Step 3. The subband with maximum texture directionality is divided into nonoverlapping blocks of size 64×64, equal to the size of the watermark.

Step 4. SVD is performed on the block that has the largest energy L^8, and the singular value matrix S of size 64×64 is obtained to achieve watermark embedding based on the rule

$$\begin{aligned} [U \ \ S \ \ V] &= \text{SVD}(L), \\ SS &= S + \alpha * W^*, \end{aligned} \tag{11}$$

where SS represents the singular value matrix containing watermarking information and α is the embedding factor used to control imperceptibility. With an increasing value of α, the amount of the embedded watermark is increased, which means that the values of SSIM (see (14)) become larger and that the distortion is more pronounced. Table 2 shows the relationship between values of α and the watermark imperceptibility in terms of SSIM.

Step 5. The watermarked image I' is obtained by the recombination of modified singular values and inverse NSST.

3.2.2. Watermark Extraction. Watermark extraction is the inverse process of watermark embedding. Note that the original image is used here to extract the watermark. The steps of watermark extraction are provided below.

Step 1. A 2-level NSST is applied to the watermarked image.

Step 2. The subband with maximum directionality is divided into nonoverlapping blocks.

Step 3. SVD is applied to the block with the largest energy L', and the singular value matrix SS' is obtained.

Step 4. The singular value matrix S is used to acquire the encrypted watermark $\widehat{W}^*$ as follows:

$$\widehat{W}^* = \frac{(SS' - S)}{\alpha}. \tag{12}$$

Step 5. The extracted watermark W' is obtained by the inverse Arnold transform in combination with key:

$$W' = \text{iarnold}\left(\widehat{W}^*, \text{key}\right). \tag{13}$$

4. Experimental Analysis

A large number of varied test images that reflect different scenes were used to test the effectiveness of the scheme. *Lena, Snow, Snow2, Plane, Baboon, Woman, Lake, Crowd, Peppers,* *Scenery, Man,* and *Bridge* (each with size 512×512) were selected as host images and a binary logo with size 64×64 was selected as the watermark (Figure 5). The "pkva" filters of NSST are used with the number of directional subbands set as 8 and 16. Also, the values of α and the secret key are set to 0.7 and 10, respectively, after numerous experimental trials. Structural similarity index measurement (SSIM) is used to measure visual quality and watermark robustness is assessed by normalized correlation (NC) and bit error rate (BER).

$$\text{SSIM}(x, y) = \frac{\left(2\mu_x\mu_y + C_1\right)\left(2\sigma_{xy} + C_2\right)}{\left(\mu_x^2 + \mu_y^2 + C_1\right)\left(\sigma_x^2 + \sigma_y^2 + C_2\right)}, \tag{14}$$

where μ_x and μ_y are the averages of x and y, σ_x^2 and σ_y^2 are the variances of x and y, and σ_{xy} is the covariance of x and y.

$$\begin{aligned} & \text{NC}\left(w, w'\right) \\ & = \frac{\sum_{i=0}^{M}\sum_{j=0}^{M} w(i, j) * w'(i, j)}{\sqrt{\sum_{i=0}^{M}\sum_{j=0}^{M} w(i, j)}\sqrt{\sum_{i=0}^{M}\sum_{j=0}^{M} w'(i, j)}}, \end{aligned} \tag{15}$$

where $w(i, j)$ represents the elements of the original watermark and $w'(i, j)$ represents the elements of the extracted watermark.

$$\text{BER} = \frac{B}{P \times Q} \times 100\%, \tag{16}$$

where B is the number of erroneously detected bits for a $P \times Q$ watermark image.

4.1. Watermarking Invisibility. The performance of the proposed algorithm was tested under no attacks. Watermark imperceptibility in terms of SSIM is shown in Table 3. SSIM values between the host and watermarked images for the proposed algorithm are greater than 0.99 and reached 1 in some images, which shows good watermark invisibility. Further, the watermark can be extracted with little distortion. NC values of the extracted watermarks are greater than 0.99 and BER values are near 0, which illustrates effective watermark extraction.

4.2. Watermarking Robustness. Tables 4–9 list the extracted watermarks for various attacks (scaling, JPEG compression, noise, and filtering) and the corresponding NC and BER values. Results show high robustness against various attacks, where the average NC and BER values are found to reach 0.985 and 0.37, respectively. The watermarking algorithm does not exhibit strong robustness for average filtering attack $(8 * 8)$ and rotation attack, for which the average NC values are 0.96 and 0.95, respectively. The performance of the watermark for various attacks is analyzed in detail in the following subsections.

4.2.1. Robustness to Scaling Attacks. Scaling operations can be used to attack a watermarked image. Table 3 shows the values of SSIM, NC, and BER for scaling attacks with scaling parameters 1/4, 1/2, 2, and 4. Figure 6 shows the extracted watermark from the attacked images *(Snow, Plane,* and *Crowd)* for a scaling parameter of 1/2.
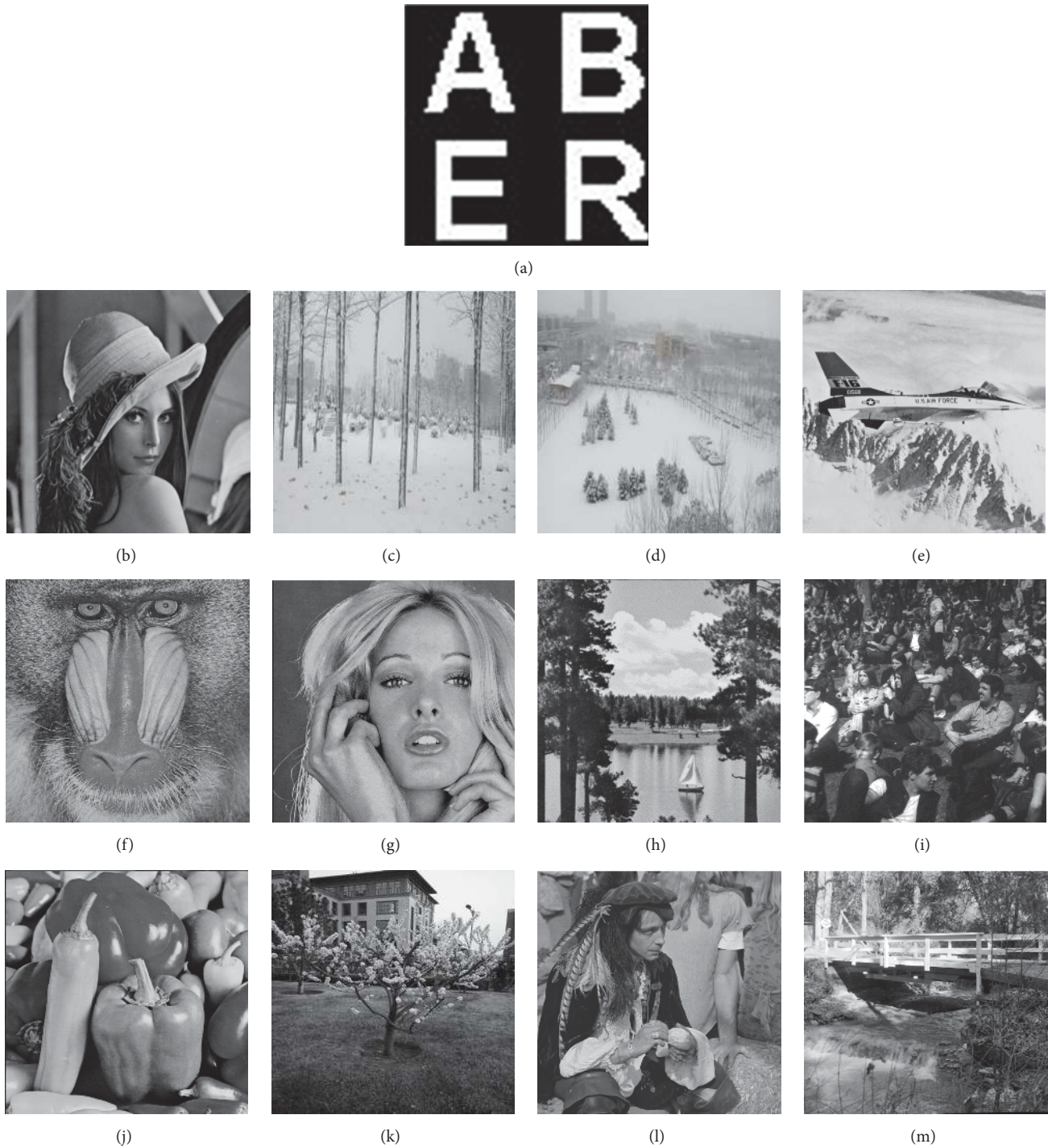
(a)

(b)   (c)   (d)   (e)

(f)   (g)   (h)   (i)

(j)   (k)   (l)   (m)

FIGURE 5: Original images: (a) *watermark image*, (b) *Lena*, (c) *Snow*, (d) *Snow2*, (e) *Plane*, (f) *Baboon*, (g) *Woman*, (h) *Lake*, (i) *Crowd*, (j) *Peppers*, (k) *Scenery*, (l) *Man*, and (m) *Bridge*.

For these test images, the extracted watermarks are clearly distinguishable. NC is greater than 0.98 and average BER is 0.8. In comparison with the other images, the result for Crowd exhibits limited robustness, but its NC value reaches 0.96, and the watermark can be extracted clearly. Therefore, the proposed algorithm can resist scaling attacks.

4.2.2. Robustness to JPEG Compression Attacks. JPEG compression is a commonly used attack in image processing. Table 5 shows the values of NC and BER for JPEG compression with different quality factors. Results suggest that, irrespective of compression factor, NC values are greater than 0.94. Therefore, the proposed algorithm is robust against

TABLE 3: Experimental results of invisibility.

Lena SSIM = 0.9997	_Snow_ SSIM = 0.9960	_Snow2_ SSIM = 0.9998	_Plane_ SSIM = 0.9990
NC/BER = 0.9961/0.1953	NC/BER = 0.9990/0.0488	NC/BER = 0.9990/0.0488	NC/BER = 0.9996/0.0268
Baboon SSIM = 0.9998	_Woman_ SSIM = 0.9995	_Lake_ SSIM = 0.9998	_Crowd_ SSIM = 0.9996
NC/BER = 0.9995/0.0244	NC/BER = 1.0000/0.0000	NC/BER = 1.0000/0.0000	NC/BER = 0.9971/0.1465
Peppers SSIM = 0.9998	_Scenery_ SSIM = 0.9997	_Man_ SSIM = 0.9990	_Bridge_ SSIM = 0.9997
NC/BER=0.9996/0.0268	NC/BER=0.9990/0.0488	NC/BER=0.9985/0.0732	NC/BER=0.9980/0.0977

TABLE 4: Experimental results for the scaling attack.

Test image	Scale = 1/4 SSIM/NC/BER	Scale = 1/2 SSIM/NC/BER	Scale = 2 SSIM/NC/BER	Scale = 4 SSIM/NC/BER
Lena	0.9599/0.9829/0.8545	0.9178/0.9702/1.4893	0.9888/0.9946/0.2686	0.9893/0.9946/0.2686
Snow	0.9056/0.9956/0.2197	0.8074/0.9961/0.1953	0.9752/0.9951/0.2441	0.9764/0.9937/0.3174
Snow2	0.9138/0.9985/0.0732	0.8248/0.9902/0.4883	0.9783/0.9985/0.0732	0.9794/0.9829/0.8545
Crowd	0.9831/0.9604/1.9775	0.9469/0.9902/0.4883	0.9960/0.9648/1.7578	0.9962/0.9834/0.8301
Woman	0.9229/0.9897/0.5127	0.8451/0.9937/0.3174	0.9793/0.9946/0.2686	0.9803/0.9951/0.2441
Lake	0.8009/0.9897/0.5127	0.6969/0.9863/0.6836	0.9373/0.9917/0.4150	0.9402/0.9922/0.3906
Plane	0.9382/0.9785/1.0742	0.8480/0.9946/0.2686	0.9851/0.9834/0.8301	0.9925/0.9634/1.8311
Baboon	0.8145/0.9961/0.1953	0.6419/0.9946/0.2686	0.9498/0.9829/0.8545	0.9523/0.9985/0.0732
Peppers	0.9131/0.9927/0.3662	0.8616/0.9922/0.3906	0.9694/0.9941/0.2930	0.9707/0.9932/0.3418
Scenery	0.7834/0.9243/3.7842	0.6043/0.9097/4.5166	0.9402/0.9727/1.3672	0.9432/0.9727/1.3672
Man	0.9526/0.9849/0.7568	0.8840/0.9897/0.5127	0.9882/0.9922/0.3906	0.9888/0.9912/0.4395
Bridge	0.9227/0.9160/4.1992	0.8152/0.9858/0.7080	0.9811/0.9888/0.5615	0.9820/0.9780/1.0986

JPEG compression. Three perfectly extracted watermarks from a JPEG attack (quality factor $Q = 40$) are shown in Figure 7.

4.2.3. Robustness to Noise Attacks. In order to evaluate the robustness of the proposed scheme against noise, every watermarked image is attacked by "Gaussian" and "Salt and Pepper" noise with variances of 0.001, 0.005, 0.01, and 0.05. Results are shown in Tables 6 and 7. For a "Gaussian" noise

attack, noise points are found to appear in the extracted watermarks when the noise variance increases. However, the extracted watermark is still distinguishable in all test images.

Similarly, for a "Salt and Pepper" noise attack, the algorithm shows good robustness. BER is 0 for _Woman_ and _Lake_ with a noise variance of 0.001, which illustrates tremendous robustness to noise attacks. Figures 8 and 9 show watermarks extracted from images attacked using "Gaussian" and "Salt and Pepper" noise with a variance of 0.001.

Table 5: Experimental results for the JPEG compression attack.

Test image	JPEG = 30 SSIM/NC/BER	JPEG = 40 SSIM/NC/BER	JPEG = 75 SSIM/NC/BER	JPEG = 90 SSIM/NC/BER
Lena	0.8752/0.9736/1.3184	0.8914/0.9751/1.2451	0.9293/0.9937/0.3174	0.9552/0.9946/0.2686
Snow	0.8477/0.9932/0.3418	0.8706/0.9980/0.0977	0.9262/0.9902/0.4883	0.9806/0.9941/0.2930
Snow2	0.8483/0.9697/1.5137	0.8723/0.9985/0.0732	0.9274/0.9985/0.0732	0.9801/0.9990/0.0488
Crowd	0.9156/0.9692/1.5381	0.9321/0.9741/1.2939	0.9658/0.9937/0.3174	0.9834/0.9688/1.5625
Woman	0.8191/0.9790/1.0498	0.8416/0.9854/0.7324	0.9041/0.9829/0.8545	0.9480/0.9937/0.3174
Lake	0.6994/0.9902/0.4883	0.7213/0.9907/0.4639	0.8199/1.0000/0.0000	0.9488/0.9858/0.7080
Plane	0.8834/0.9409/2.9541	0.9024/0.9458/2.7100	0.9432/0.9688/1.5625	0.9666/0.9717/1.4160
Baboon	0.7598/0.9976/0.1221	0.7905/0.9976/0.1221	0.8777/0.9028/4.8548	0.9748/0.9995/0.0244
Peppers	0.8158/0.9600/2.0020	0.8336/0.9785/1.0742	0.8771/0.9863/0.6836	0.9227/0.9932/0.3418
Scenery	0.7682/0.9546/2.2705	0.8117/0.9761/1.1963	0.9334/0.9780/1.0986	0.9837/0.9897/0.5127
Man	0.8646/0.9844/0.7813	0.8857/0.9863/0.6836	0.9364/0.9917/0.4150	0.9682/0.9922/0.3906
Bridge	0.8650/0.9546/2.2705	0.8868/0.9619/1.9043	0.9435/0.9717/1.4160	0.9795/0.9780/1.0986

Table 6: Experimental results for the "Gaussian" white noise attack.

Test image	Var = 0.001 SSIM/NC/BER	Var = 0.005 SSIM/NC/BER	Var = 0.01 SSIM/NC/BER	Var = 0.05 SSIM/NC/BER
Lena	0.6183/0.9960/0.2209	0.3432/0.9951/0.2441	0.2481/0.9932/0.3418	0.0989/0.9907/0.4639
Snow	0.6721/0.9941/0.2930	0.4617/0.9897/0.5127	0.3710/0.98191/0.9033	0.3709/0.9751/1.2451
Snow2	0.6239/0.9985/0.0732	0.3641/0.9966/0.1709	0.2643/0.9912/0.4395	0.1009/0.9883/0.5859
Crowd	0.7400/0.9971/0.1465	0.5013/0.9956/0.2197	0.3962/0.9951/0.2441	0.1869/0.9941/0.2930
Woman	0.6985/0.9980/0.0977	0.4140/0.9961/0.1953	0.3029/0.9951/0.2441	0.1217/0.9893/0.5371
Lake	0.8259/0.9946/0.2686	0.5657/0.9937/0.3174	0.4452/0.9922/0.3906	0.2147/0.9917/0.4150
Plane	0.6115/0.9785/1.0742	0.8480/0.9946/0.2686	0.9851/0.9834/0.8301	0.9925/0.9634/1.8311
Baboon	0.8925/0.9858/0.7080	0.3671/0.9854/0.7324	0.2853/0.9814/0.9277	0.1389/0.9805/0.9766
Peppers	0.6661/0.9966/0.1709	0.3805/0.9902/0.4883	0.2802/0.9897/0.5127	0.1190/0.9717/1.4160
Scenery	0.8961/0.9961/0.1953	0.7407/0.9956/0.2197	0.6310/0.9883/0.5859	0.3370/0.9780/1.0986
Man	0.7385/0.9951/0.2441	0.4691/0.9941/0.2930	0.3514/0.9922/0.3906	0.1454/0.9917/0.4150
Bridge	0.8812/0.9980/0.0977	0.6653/0.9961/0.1953	0.5342/0.9951/0.2441	0.2471/0.9717/1.4160

Table 7: Experimental results for the "Salt and Pepper" noise attack.

Test image	Var = 0.001 SSIM/NC/BER	Var = 0.005 SSIM/NC/BER	Var = 0.01 SSIM/NC/BER	Var = 0.05 SSIM/NC/BER
Lena	0.9634/0.9961/0.1953	0.8350/0.9951/0.2441	0.6992/0.9927/0.3662	0.2601/0.9893/0.5371
Snow	0.9750/0.9995/0.0244	0.8720/0.9941/0.2930	0.7585/0.9849/0.7568	0.3737/0.9795/1.0254
Snow2	0.9664/0.9990/0.0488	0.8484/0.9985/0.0732	0.7226/0.9980/0.0977	0.2806/0.9976/0.1221
Crowd	0.9739/0.9956/0.2197	0.8822/0.9941/0.2930	0.7835/0.9893/0.5371	0.4001/0.9727/1.3672
Woman	0.9669/1.0000/0.0000	0.8406/0.9985/0.0732	0.7232/0.9951/0.2441	0.3120/0.9946/0.2686
Lake	0.9799/1.0000/0.0000	0.8931/0.9927/0.3662	0.8074/0.9771/1.1475	0.4327/0.9771/1.1475
Plane	0.9630/0.9990/0.0488	0.8441/0.9985/0.0732	0.7197/0.9829/0.8545	0.3028/0.9751/1.2451
Baboon	0.9826/0.9995/0.0244	0.9146/0.9868/0.6592	0.8416/0.9849/0.7568	0.5131/0.9834/0.8301
Peppers	0.9597/0.9990/0.0488	0.8392/0.9941/0.2930	0.7190/0.9897/0.5127	0.2929/0.9795/1.0254
Scenery	0.9860/0.9937/0.3174	0.9363/0.9888/0.5615	0.8779/0.9600/2.0020	0.5842/0.9580/2.0996
Man	0.9685/0.9985/0.0732	0.8655/0.9956/0.2197	0.7591/0.9922/0.3906	0.3522/0.9766/1.1719
Bridge	0.9816/0.9956/0.2197	0.9150/0.9888/0.5615	0.8383/0.9785/1.0742	0.5042/0.9717/1.4160

TABLE 8: Experimental results for the filtering attack.

Test image	Average filtering (4 ∗ 4) SSIM/NC/BER	Average filtering (8 ∗ 8) SSIM/NC/BER	Median filtering (3 ∗ 3) SSIM/NC/BER	Median filtering (4 ∗ 4) SSIM/NC/BER
Lena	0.8963/0.9897/0.5127	0.6256/0.9888/0.5615	0.9171/0.9893/0.5371	0.8560/0.9927/0.3662
Snow	0.7918/0.9937/0.3174	0.5378/0.9849/0.7568	0.8142/0.9946/0.2686	0.7938/0.9854/0.7324
Snow2	0.8140/0.9956/0.2197	0.5604/0.9795/1.0254	0.8022/0.9985/0.0732	0.7287/0.9976/0.1221
Crowd	0.9528/0.9517/2.4170	0.6273/0.9517/2.4170	0.9581/0.9717/1.4160	0.8739/0.9937/0.3174
Woman	0.8149/0.9888/0.5615	0.5439/0.9878/0.6104	0.8450/0.9946/0.2686	0.9803/0.9951/0.2441
Lake	0.5161/0.9604/1.9775	0.3495/0.9580/2.0996	0.6287/0.9907/0.4639	0.6084/0.9917/0.4150
Plane	0.9335/0.9990/0.0488	0.6509/0.9736/1.3184	0.9391/0.9985/0.0732	0.8734/0.9619/1.9043
Baboon	0.5440/0.9966/0.1709	0.3143/0.9858/0.7080	0.6062/0.9971/0.1465	0.4693/0.9951/0.2441
Peppers	0.7599/0.9858/0.7080	0.5429/0.9795/1.0254	0.8605/0.9941/0.2930	0.8082/0.9937/0.3174
Scenery	0.4698/0.9600/2.0020	0.2828/0.9590/2.0508	0.5736/0.9897/0.5127	0.4622/0.9727/1.3672
Man	0.8802/0.9834/0.8301	0.5707/0.9785/1.0742	0.8957/0.9946/0.2686	0.7916/0.9546/2.2705
Bridge	0.8086/0.9771/1.1475	0.4776/0.9717/1.4160	0.8205/0.9937/0.3174	0.6796/0.9907/0.4639

TABLE 9: Experimental results for the rotation attack.

Test image	Angle = 5° SSIM/NC/BER	Angle = 10° SSIM/NC/BER	Angle = 15° SSIM/NC/BER	Angle = 30° SSIM/NC/BER
Lena	0.3521/0.9907/0.4639	0.2733/0.9795/1.0254	0.2501/0.9624/1.8799	0.2200/0.9473/2.6367
Snow	0.2879/0.9717/1.4160	0.2565/0.9702/1.4893	0.2301/0.9688/1.5625	0.1901/0.9639/1.8066
Snow2	0.3586/0.9736/1.3184	0.3025/0.9639/1.8066	0.2736/0.9517/2.4170	0.2141/0.9409/2.9541
Crowd	0.1649/0.9814/0.9277	0.1191/0.9800/1.0010	0.1102/0.9692/1.5381	0.0822/0.9404/2.9785
Woman	0.2764/0.9902/0.4883	0.1928/0.9863/0.6836	0.1554/0.9727/1.3672	0.1440/0.9556/2.2217
Lake	0.1045/0.9761/1.1963	0.0882/0.9741/1.2939	0.0814/0.9727/1.3672	0.0656/0.9390/3.0518
Plane	0.3484/0.9810/0.9521	0.2872/0.9785/1.0742	0.2615/0.9673/1.6357	0.2293/0.9600/2.002
Baboon	0.0800/0.9863/0.6836	0.0635/0.9814/0.9277	0.0540/0.9756/1.2207	0.0454/0.9546/2.2705
Peppers	0.2760/0.9858/0.7080	0.2076/0.9780/1.0986	0.1786/0.9717/1.4160	0.1453/0.9590/2.0508
Scenery	0.0817/0.9863/0.6836	0.0598/0.9844/0.7813	0.0470/0.9814/0.9277	0.0287/0.9756/1.2207
Man	0.1871/0.9897/0.5127	0.1435/0.9893/0.5371	0.1165/0.9785/1.0742	0.0994/0.9600/2.0020
Bridge	0.0584/0.9961/0.1953	0.0461/0.9653/1.7334	0.0418/0.9580/2.0996	0.0369/0.9546/2.2705

4.2.4. Robustness to Filtering Attacks. As shown in Table 8, for both average and median filtering, the extracted watermarks are distinguishable in the test images. Three examples are presented in Figure 10 for a 3×3 median filtering attack. SSIM values of the watermarked image suggest that the image is easily distorted by the filtering attack. However, average NC is 0.975 and BER is 0.8, which illustrates that the proposed algorithm can resist the filtering attack.

4.2.5. Robustness to Rotation Attacks. The watermark is embedded into the most obvious directional subband. As shown by the SSIM values in Table 9, the loss of information is significant when the image is rotated. In order to illustrate the ability to resist a rotation attack, watermarked images are rotated by 5°, 10°, 15°, and 30°. With an increase in rotation angle, the quality of the extracted watermark is reduced. The average NC value is 0.95. Compared with other forms of image attacks, the quality of the extracted watermark is poorer. Figure 11 shows watermarks extracted from images attacked using rotation attack with 15°.

4.3. Comparative Analysis. In this section, the proposed algorithm is compared with methods based on the discrete wavelet transform domain (DWT-SVD) [20], nonsubsample contourlet transform domain (NSCT-SVD) [12], and shearlet transform domain (ST-SVD) [17]. Tables 10 and 11 and Figures 12 and 13 show a comparison of robustness for certain attacks on the four methods. The line chart indicates that NC values of the proposed NSST-SVD technique are the largest among the three methods for noise and filtering attacks. This enhancement in performance highlights the optimal nature of the shearlet transform for digital watermarking. NC for JPEG and scaling attacks is only marginally lower for the proposed algorithm compared to the others. Overall, the proposed algorithm displays noteworthy performance.

FIGURE 6: Extracted watermarks from attacked images *(Snow, Plane,* and *Crowd)* after a scaling attack (scale = 1/2).

FIGURE 7: Extracted watermarks from attacked images *(Snow, Plane,* and *Crowd)* after a JPEG attack (JPEG = 40).

FIGURE 8: Extracted watermarks from attacked images *(Snow, Plane,* and *Crowd)* after a "Gaussian" noise attack (Var = 0.001).

FIGURE 9: Extracted watermarks from attacked images *(Snow, Plane,* and *Crowd)* after a "Salt and Pepper" noise attack (Var = 0.001).

FIGURE 10: Extracted watermarks from attacked images *(Snow, Plane,* and *Crowd)* after a median filtering attack (3 ∗ 3).

TABLE 10: Comparison of NC values on *Lena* image.

Attacks	Comparison of NC values for four schemes			
	DWT-SVD	NSCT-SVD	Ref. [17]/ST-SVD	Proposed/NSST-SVD
(1) JPEG ($Q = 40$)	0.9971	1.0000	0.9938	0.9751
(2) Gaussian noise (Var = 0.001)	0.7673	0.9683	0.9859	0.9960
(3) Salt and Pepper (Var = 0.001)	0.8268	0.9554	0.9622	0.9961
(4) Scaling (scale = 1/4)	0.9354	0.9866	0.9427	0.9829
(5) Average filtering ($8 * 8$)	0.9156	0.9731	0.9182	0.9888
(6) Median filtering ($4 * 4$)	0.9980	0.9321	0.9718	0.9927

TABLE 11: Comparison of NC values on *Baboon* image.

Attacks	Comparison of NC values for four schemes			
	DWT-SVD	NSCT-SVD	Ref. [17]/ST-SVD	Proposed/NSST-SVD
(1) JPEG ($Q = 40$)	0.9880	0.9983	0.9926	0.9976
(2) Gaussian noise (Var = 0.001)	0.8989	0.9739	0.9718	0.9858
(3) Salt and Pepper (Var = 0.001)	0.8416	0.9747	0.9934	0.9995
(4) Scaling (scale = 1/4)	0.9441	0.9968	0.8742	0.9961
(5) Average filtering ($8 * 8$)	0.9222	0.9801	0.8467	0.9858
(6) Median filtering ($4 * 4$)	0.9803	0.9557	0.8936	0.9951

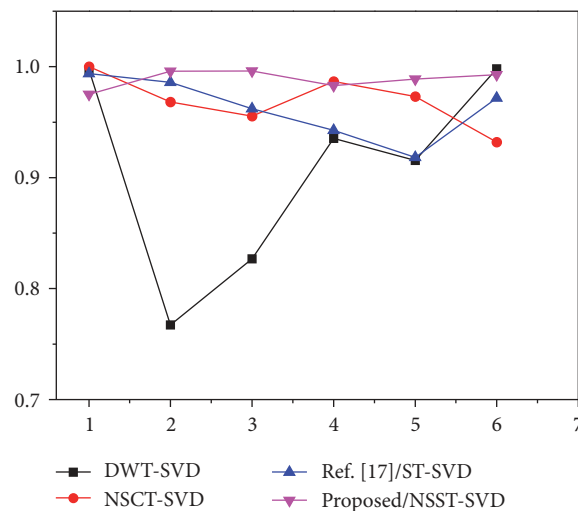FIGURE 11: Extracted watermarks from attacked images *(Snow, Plane,* and *Crowd)* after a rotation attack (15°).

FIGURE 12: Comparison of NC for four algorithms on *Lena* image.

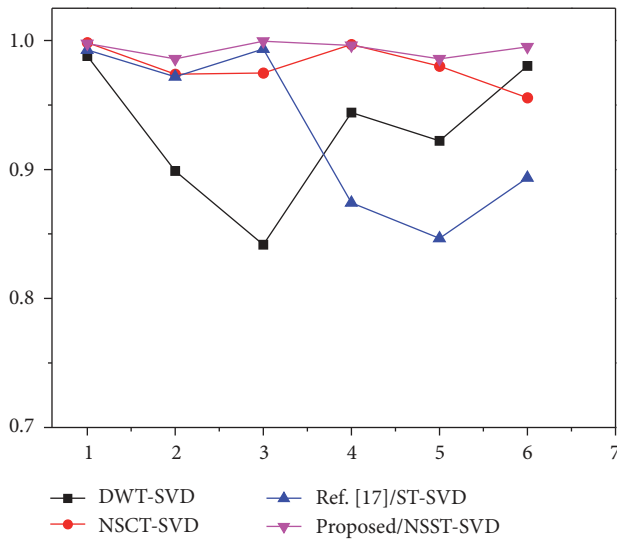FIGURE 13: Comparison of NC for four algorithms on *Baboon* image.

Legend:
- ■ DWT-SVD
- ▲ Ref. [17]/ST-SVD
- ● NSCT-SVD
- ▼ Proposed/NSST-SVD

5. Conclusions

A novel watermarking algorithm based on texture directionality was proposed by combining the advantages of the non-subsample shearlet and singular value decomposition. The strongest directionality subband, which provides the most significant texture information of the image, was selected for embedding the watermark since it preserves perceptual image quality. The proposed scheme is found to exhibit noteworthy robustness for most image processing attacks such as noise, rotation, cropping, and filtering. A comparison with two existing hybrid watermarking techniques showed better performance of the proposed method for many of the tested attacks.

Conflicts of Interest

The authors declare no competing financial interests regarding the publication of this paper.
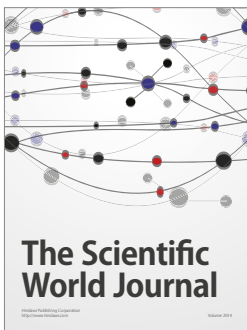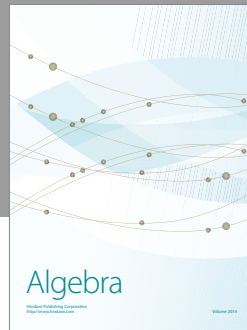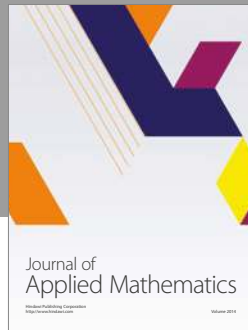
Acknowledgments

References

[1] J. Fridrich, "Applications of data hiding in digital images," in *Proceedings of the Fifth International Symposium on Signal Processing and Its Applications*, Queensland, Australia.

[2] N. Bansal, V. K. Deolia, A. Bansal, and P. Pathak, "Digital image watermarking using least significant bit technique in different bit positions," in *Proceedings of the 2014 6th International Conference on Computational Intelligence and Communication Networks, CICN 2014*, pp. 813–818, Bhopal, India, 2014.

[3] M. Cedillo-Hernandez, F. Garcia-Ugalde, M. Nakano-Miyatake, and H. Perez-Meana, "Robust object-based watermarking using SURF feature matching and DFT domain," *Radioengineering*, vol. 22, no. 4, pp. 1057–1071, 2013.

[4] Q. Su, G. Wang, S. Jia, X. Zhang, Q. Liu, and X. Liu, "Embedding color image watermark in color image based on two-level DCT," *Signal, Image and Video Processing*, vol. 9, no. 5, pp. 991–1007, 2015.

[5] A. Mishra, C. Agarwal, A. Sharma, and P. Bedi, "Optimized gray-scale image watermarkingusing DWT-SVD and firefly algorithm," *Expert Systems with Applications*, vol. 41, no. 17, pp. 7858–7867, 2014.

[6] M. Benouaret, A. Sahour, and S. Harize, "Real time implementation of a signal denoising approach based on eight-bits DWT," *AEU—International Journal of Electronics and Communications*, vol. 66, no. 11, pp. 937–943, 2012.

[7] H. Sadreazami and M. Amini, "A robust spread spectrum based image watermarking in ridgelet domain," *AEU—International Journal of Electronics and Communications*, vol. 66, no. 5, pp. 364–371, 2012.

[8] T. Wang and H. Li, "A novel scrambling digital image watermark algorithm based on double transform domains," *Mathematical Problems in Engineering*, vol. 2015, Article ID 937432, 13 pages, 2015.

[9] H. Bi, Y. Liu, M. Wu, and Y. Ge, "NSCT domain additive watermark detection using RAO hypothesis test and cauchy distribution," *Mathematical Problems in Engineering*, vol. 2016, Article ID 4065215, 18 pages, 2016.

[10] J. Liu, G. Liu, W. He, and Y. Li, "A new digital watermarking algorithm based on WBCT," *Procedia Engineering*, vol. 29, pp. 1559–1564, 2012.

[11] F. Rahimi and H. Rabani, "A visually imperceptible and robust image watermarking scheme in contourlet domain," in *Proceedings of the 2010 IEEE 10th International Conference on Signal Processing, ICSP2010*, pp. 1817–1820, Beijing, China, 2010.

[12] S.-M. Zhu and J.-M. Liu, "Novel blind watermarking scheme in contourlet domain based on singular value decomposition," in *Proceedings of the 2nd International Workshop on Knowledge Discovery and Data Mining (WKKD '09)*, pp. 672–675, Moscow, Russia, 2009.

[13] G. Easley, D. Labate, and W.-Q. Lim, "Sparse directional image representations using the discrete shearlet transform," *Applied and Computational Harmonic Analysis. Time-Frequency and Time-Scale Analysis, Wavelets, Numerical Algorithms, and Applications*, vol. 25, no. 1, pp. 25–46, 2008.

[14] P. Kittipoom, G. Kutyniok, and W.-Q. Lim, "Construction of compactly supported shearlet frames," *Constructive Approximation. An International Journal for Approximations and Expansions*, vol. 35, no. 1, pp. 21–72, 2012.

[15] B. Ahmederahgi, F. Kurugollu, P. Milligan, and A. Bouridane, "Spread spectrum image watermarking based on the discrete shearlet transform," in *Proceedings of the 4th European Workshop on Visual Information Processing (EUVIP '13)*, pp. 178–183, Paris, France, June 2013.

[16] J. Zhao, M. Sun, J. Jia, L. Huang, F. Han, and S. Liu, "Image watermark based on extended shearlet and insertion using the largest information entropy on horizontal cone," *Mathematical Problems in Engineering*, vol. 2015, Article ID 450819, 10 pages, 2015.

[17] M. Mardanpour and M. A. Z. Chahooki, "Robust transparent image watermarking with Shearlet transform and bidiagonal singular value decomposition," *AEU—International Journal of Electronics and Communications*, vol. 70, no. 6, pp. 790–798, 2016.

[18] X. Wang, Y. Liu, S. Li, H. Yang, and P. Niu, "Robust image watermarking approach using polar harmonic transforms based geometric correction," *Neurocomputing*, vol. 174, pp. 627–642, 2016.

[19] C.-C. Lin, C.-C. Chang, and Y.-H. Chen, "A novel SVD-based watermarking scheme for protecting rightful ownership of digital images," *Journal of Information Hiding and Multimedia Signal Processing*, vol. 5, no. 2, pp. 124–143, 2014.

[20] R. Mehta and N. Rajpal, "A hybrid semi-blind gray scale image watermarking algorithm based on DWT-SVD using human visual system model," in *Proceedings of the 6th International Conference on Contemporary Computing, (IC3 '13)*, pp. 163–168, Noida, India, 2013.

[21] B. L. Gunjal and S. N. Mali, "MEO based secured, robust, high capacity and perceptual quality image watermarking in DWT-SVD domain," *SpringerPlus*, vol. 4, no. 1, pp. 1–16, 2015.

[22] A. Benhocine, L. Laouamer, L. Nana, and A. C. Pascu, "New images watermarking scheme based on singular value decomposition," *Journal of Information Hiding and Multimedia Signal Processing*, vol. 4, no. 1, pp. 9–18, 2013.

[23] K. Loukhaoukha, "On the security of digital watermarking scheme based on SVD and tiny-GA," *Journal of Information Hiding and Multimedia Signal Processing*, vol. 3, no. 2, pp. 135–141, 2012.

[24] M. M. Islam, D. Zhang, and G. Lu, "A geometric method to compute directionality features for texture images," in *Proceedings of the IEEE International Conference on Multimedia and Expo, (ICME '08)*, pp. 1521–1524, Hannover, Germany, 2008.

[25] Y.-W. Kim and I.-S. Oh, "Watermarking text document images using edge direction histograms," *Pattern Recognition Letters*, vol. 25, no. 11, pp. 1243–1251, 2004.